Modeling non-stationary, non-axisymmetric heat patterns in DIII-D tokamak

D. Ciro[1], T. E. Evans[2], I. L. Caldas[3*]
[1,3] *Department of Applied Physics, São Paulo University, São Paulo, CEP 05508-090, Brazil*
[2] *General Atomics, PO Box 85608, San Diego, CA 92186-5608, USA.*

Non-axisymmetric stationary magnetic perturbations lead to the formation of homoclinic tangles near the divertor magnetic saddle in tokamak discharges. These tangles intersect the divertor plates in static helical structures that delimit the regions reached by open magnetic field lines reaching the plasma column and leading the charged particles to the strike surfaces by parallel transport. In this article we introduce a non-axisymmetric rotating magnetic perturbation to model the time development of the three-dimensional magnetic field of a single-null DIII-D tokamak discharge developing a rotating tearing mode. The stable and unstable manifolds of the asymmetric magnetic saddle are calculated through an adaptive method providing the manifold cuts at a given poloidal plane and the strike surfaces. For the modeled shot, the experimental heat pattern and its time development are well described by the rotating unstable manifold, indicating the emergence of homoclinic lobes in a rotating frame due to the plasma instabilities. In the model it is assumed that the magnetic field is created by a stationary axisymmetric plasma current and a set of rotating internal helical filamentary currents. The currents in the filaments are adjusted to match the waveforms of the magnetic probes at the mid-plane and the rotating magnetic field is introduced as a perturbation to the axisymmetric field obtained from a Grad-Shafranov equilibrium reconstruction code.

I. INTRODUCTION

In single-null, axisymmetric, tokamak discharges the plasma becomes limited by a homoclinic magnetic separatrix. Such magnetic surface is not resilient in three dimensions [1], and, formally, any departure from axisymmetry will lead to the splitting of the magnetic separatrix into two different surfaces named invariant manifolds. These surfaces intersect each other innumerable times as they are stretched and folded in the neighborhood of the X-points [1–3]. The existence of these non-axisymmetric structures has been demonstrated experimentally by measuring the heat deposition patterns in the divertor tiles [4], or by tangential imaging of the X-point region [5], and is a subject of discussion since the observation of helical footprints in tokamak discharges [6].

Modeling the interaction of the internal non-axisymmetric currents with the magnetic separatrix in single-null discharges is important to understand the influence of the plasma instabilities on the heat deposition in the divertor tiles. In ITER discharges a rotating non-axisymmetric divertor heat flux will cause periodic variation in the thermal loading of the target plates and cooling lines resulting in thermal and mechanical fatigue of these components leading to premature failures. This type of slowly rotating non-axisymmetric internal mode must be controlled to prevent damage to the divertor.

Experiments using internal 3D coils, such as those being installed in ITER, have been carried out in DIII-D to entrain these modes and prevent them from resulting in disruptions [7], but additional research is needed to better understand how to mitigate the thermal cycling of the divertors and this involves modeling the time-dependent evolution of the heat patterns caused by the internal modes.

To understand the formation of these patterns we need to appeal to the divergence-free nature of the magnetic field. In this context, the magnetic field lines are described by a three-dimensional Hamiltonian system with one of the spatial coordinates being the independent variable. In magnetically diverted configurations the field lines starting near the plasma edge intersect the divertor targets in static spiral regions in agreement with the experimental heat deposition patterns [8]. These patterns are organized by the invariant manifolds of the field lines.

In more general situations the magnetic field changes in time, and, formally, the Hamiltonian function must be redefined at each instant. For these cases the system becomes four-dimensional and the magnetic invariants must evolve in time. However, in the special case in which the magnetic perturbation rotates toroidally we can calculate the invariants in a rotating frame and then recover the temporal evolution in the laboratory frame. Experimental observations of heat deposition patterns consistent with the rigid rotation of an invariant manifold have been pointed in [4], where the measured magnetic perturbation was due to a slowly rotating $q = 2$ tearing mode. In this work, we show the quantitative agreement between the measured heat flux profiles at the divertor tiles and the area delimited by the unstable invariant manifold calculated for the DIII-D in a single-null discharge.

In the discharge #158826, the Electron Cyclotron Emission (ECE) signal reverses its phase at $q = 2$, indicating the presence of a tearing island, and it is well correlated with the measured magnetic signals outside the plasma column. The slowly growing tearing mode is observed to rotate toroidally at an approximately constant rate. To model the non-axisymmetric field produced by

* [1]davidcirotaborda@usp.br
[2]evans@fusion.gat.com
[3]ibere@if.usp.br

the helical modes at $q = 2$ we consider a set of helical filamentary currents resting at an internal magnetic surface of the EFIT axisymmetric equilibrium reconstruction of the shot [9]. This approach is similar to the one used to model the plasma response to applied Resonant Magnetic Perturbations (RPMs) in COMPASS-D [8, 10]. However, in this situation, we do not prescribe the filaments using the X and O points induced by the RMPs, as this is inconvenient due to the proximity of the surface $q = 2$ to the plasma edge. Conversely, we define our filaments in more internal surfaces to avoid undesired effects due to the discretization of the response currents.

A more sophisticated approach involves modeling the equilibrium with fully three-dimensional solvers using energy minimization procedures. However, most tractable procedures extremize the plasma potential energy by performing ideal variations of the magnetic field, precluding topological changes at the resonant surfaces and the plasma edge [11]. This, in turn, preserves numerically the nested topology, and prevents the experimentally observed separatrix splitting.

To avoid such difficulties we do not solve the self-consistent plasma equilibrium but model the plasma dynamics and response by adjusting the currents, phases and toroidal rotation frequency of the model filaments. This is done using a functional minimization procedure that reaches the optimum configuration when the model reproduce the magnetic measurements at the mid-plane probes of DIII-D.

Since the non-axisymmetric components of the plasma current are not concentrated in filaments, this method is only reasonable if the modeled perturbation source is far from the place where we study its effects. Once we obtain the perturbation field we calculate the magnetic invariants in the rotating frame using a method similar to the described in [12], then we recover the expected time-dependent region delimited by the manifold in the laboratory frame. The calculated manifold interior is in good agreement with the time-dependent heat flux profiles measured at the divertor plates in a fixed toroidal position.

The calculations of the invariant manifolds presented in this work are performed with the MAGMAN routine, which involves the determination of the Unstable Periodic Orbit (UPO) that generalizes the X-point in three dimensional situations. This routine returns the manifolds as an ordered well-spaced sequence of points in the desired cut on the tokamak chamber. This method is preferred over the laminar plots, as is computationally efficient and delimits naturally the abrupt transitions in the connection lengths, also, it can be naturally generalized to represent the manifolds as delimiting surfaces in three-dimensions, which is relevant for inherently non-stationary non-axisymmetric configurations like the one presented here.

This manuscript is organized as follows. In Section II we present a summary of the experimental observations of the DIII-D discharge #158826. In Section III we introduce the filamentary currents model and adjust its parameters to match the measured magnetic fluctuations and calculate the corresponding invariant manifolds for the equilibrium reconstruction. In Section IV we present our main result, namely the correspondence between the internal region delimited by the unstable manifold, and the measured time-dependent heat flux at the divertor tiles. Finally, in Section V we present our conclusions and perspectives, and we included some technical details on the manifold calculations in the Appendix.

II. EXPERIMENTAL OBSERVATIONS

The basic evidence of the interplay between the magnetic topology and the plasma edge, or, even, the definition of the plasma edge through the invariant manifolds, is the temporal correlation between the magnetic fluctuations at the magnetic probes and the evolution of the heat-flux pattern in the Plasma Facing Components (PFCs).

In this work, we consider the discharge #158826 of DIII-D where a small stationary $n = 2$ field was applied. A non-rotating locked mode forms at 1625 ms and remains stationary until 2015 ms when it begins to rotate slowly at approximately 6.67 Hz. During the non-rotating phase two heat flux peaks form at the outer strike point and remain fixed until the mode begins to rotate.

In Fig. 1 we show the poloidal magnetic field fluctuations at different toroidal positions in the Low Field Side (LFS) mid-plane and the corresponding measurements of the heat flux from an IR camera pointing to the lower divertor region during the rotating stage. As the magnetic signals complete one cycle, the heat flux profile completes one bifurcation cycle, where a single peak splits into two or three peaks that move to the LFS and vanish.

This type of behavior is expected if the non-axisymmetric field created by an internal instability is changing periodically the magnetic topology, resulting in a periodic separation of the strike points measured by the IR camera [4].

In this shot Electron Cyclotron Emission presents a phase inversion across the $q = 2$ surface indicating the presence of a tearing island. Also, the modulation in the radial and poloidal magnetic fields measured at several toroidal positions for the same poloidal location are consistent with a $q = 2$ tearing mode rotating at approximately 6.67 Hz. The amplitude of the mode grows slowly, but it is modeled to be constant during the heat flux measurements. It is important to point out that although the phase differences between the signals are consistent with the rigid rotation of the mode, the waveforms captured at different toroidal locations present different shapes, indicating that the internal structure is not rotating rigidly, but may contain elements moving at different frequencies or even oscillating. However, these effects are not included in the model as they do not introduce informa-

tion that can be resolved with the IR camera, also, the dominant mode provides substantial agreement with the available experimental data.

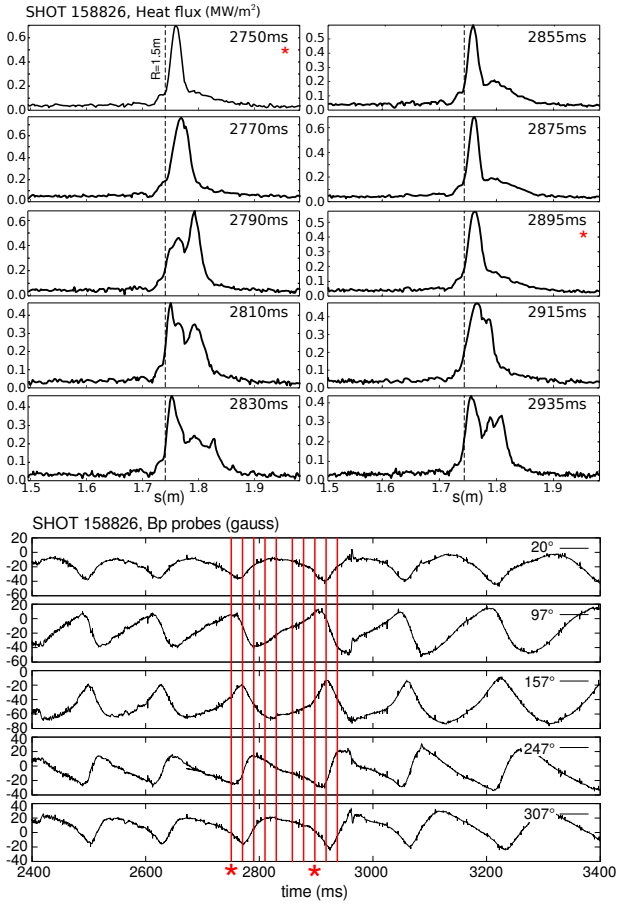

FIG. 1. Heat flux profiles in the LFS strike point for discharge #158826 for ten time slices between 2750 ms and 2935 ms (top) and poloidal magnetic field differences between various toroidal positions measured on the LFS mid-plane (bottom). The dashed lines in the heat flux profiles identify the strike point position obtained from the EFIT reconstruction of the discharge, the red lines identify the times for the heat profile measurements and the asterisks denote heat measurements separated by almost one complete period (150 ms) of the magnetic signals. The coordinate s in the heat flux profiles corresponds to the poloidal distance along the DIII-D wall, measured counterclockwise from the HFS mid-plane. For these profiles $s = R + 0.239$ m, with R the cylindrical radial coordinate.

III. PERTURBATION AND SEPARATRIX

A. Helical filaments model for the perturbation

In order to show a clear correlation between the magnetic signals and the divertor heat flux we will concentrate in modeling the time-dependent part of the magnetic field, which agrees experimentally with the heat flux becoming non-stationary. For this, we split the total magnetic field in the form

$$\vec{B}(\vec{r},t) = \vec{B}_0(\vec{r}) + \vec{B}_1(\vec{r},t). \tag{1}$$

In the discharge #158826, the stationary $n = 2$ field is small compared to the magnetic fluctuations, consequently, the stationary part $\vec{B}_0$, is considered to be axisymmetric and was obtained from an EFIT equilibrium reconstruction of the discharge [9]. This Grad-Shafranov solution assumes a two-dimensional equilibrium, and solves the inverse problem of finding the plasma profiles for the measured plasma parameters.

For the non-axisymmetric part, we introduce the time-dependent field $\vec{B}_1(\vec{r},t)$, which is considered to be periodic in time and produced by the plasma alone. If the perturbed field is produced by a rotating, non-axisymmetric current distribution inside the plasma, there is a stationary magnetic perturbation $\vec{B}'_1(R',z',\phi')$ in the reference frame rotating around z with angular velocity $2\pi/T$. As we are dealing with a slow fluctuation with an approximate frequency of $1/T \sim 6.67$ Hz, we can approximate the magnetic field in the rotating frame by

$$\vec{B}'_1(R',z',\phi') = \vec{B}_1(R,z,\phi - 2\pi t/T), \tag{2}$$

where $\phi' = \phi - 2\pi t/T$ is the azimuthal angle in the rotating frame and the cylindrical coordinates (R,z) are unaffected by the coordinate transformation. If this is fulfilled, we can study the three-dimensional problem of the stationary magnetic field in the rotating frame, and recover the spatio-temporal dynamics in the laboratory frame to compare with the experimental observations.

To model the perturbing field we consider an internal set of helical filaments, carrying the non-axisymmetric currents inside the plasma and use the magnetic measurements at different angular positions to set the current and phase of each filament. This simple approach allow us to mimic the experimental behavior of the system without resorting to MHD calculations. For a set of N_f filaments with helicity q_h on the magnetic surface with safety factor q, the non-axisymmetric part of the current density inside the plasma takes the form

$$\vec{j}_1(\vec{r},t) = \sum_{i=1}^{N_f} I_i \delta(\vec{r} - \vec{r}_h(\phi_i - \Omega t))\hat{h}, \tag{3}$$

where I_i is the current of the i'th filament, $\hat{h}$ is the current direction at $\vec{r}$ and $\vec{r}_h(\phi_0)$ is a helix with q_h toroidal turns per poloidal turn. The desired helical path is obtained by appropriate scaling of the toroidal coordinate of a discretized field line starting at the toroidal angle ϕ_0 on the LFS mid-plane at the magnetic surface q, so that the line helicity becomes q_h.

For the DIII-D discharge #158826 a tearing mode develops at the $q = 2$ surface which is at approximately 8 cm from the separatrix at the LFS. Placing the helical filaments at this location allows us to model the measured magnetic fluctuations in the probes. However, due

to the small distance between the filaments and the separatrix, the discrete nature of the helical currents cause undesired topological effects, as the deformation of the manifold around the filaments. Consequently, we do not use field aligned filaments at $q = 2$, but consider three filaments with $q_h = 2$ at the more internal surface $q = 1$, located at a larger distance to the separatrix (~ 34 cm for the LFS midplane).

Our approximations are only applicable for studying the perturbed field lines outside the magnetic surfaces where the instability is formed, and are not intended to model the internal magnetic islands self-consistently, this is why we have freedom to locate the perturbation sources in different locations, whenever we can reproduce the measured magnetic fluctuations.

The current in the filaments $\{I_1, I_2, I_3\}$ and their toroidal phases $\{\phi_1, \phi_2, \phi_3\}$ are determined simultaneously using a Levenberg-Marquardt routine [13] to minimize the corresponding error functional

$$\epsilon(\{I_i, \phi_i\}) = \sum_{k=1}^{N} [\tilde{B}_z(t_k) - B_1(\{I_i, \phi_i\}, \Omega t_k)]^2. \qquad (4)$$

Where $\tilde{B}_z(t)$ is the measured vertical field fluctuation for a given of magnetic probe at the time t, and $\{t_k\}$ are N equally spaced time slices of the desired time interval. The simulated magnetic perturbation $B_1(\{I_i, \phi_i\}, \phi)$ is calculated for the corresponding angles, $\phi_k = \Omega t_k$, in the rotating frame, where $\Omega = 2\pi \times 6.67$Hz is the measured toroidal rotation frequency, and the adjusted time interval corresponds to the heat measurements in Fig. 1. When provided a reasonable initial guess for the parameters, the routine converges to a minimum value of the error, where $\{I_1, I_2, I_3\} = \{2.27, 32.21, -29.88\}$ kA and $\{\phi_1, \phi_2, \phi_3\} = \{58.2°, 127.2°, 166.16°\}$ (Fig. 2).

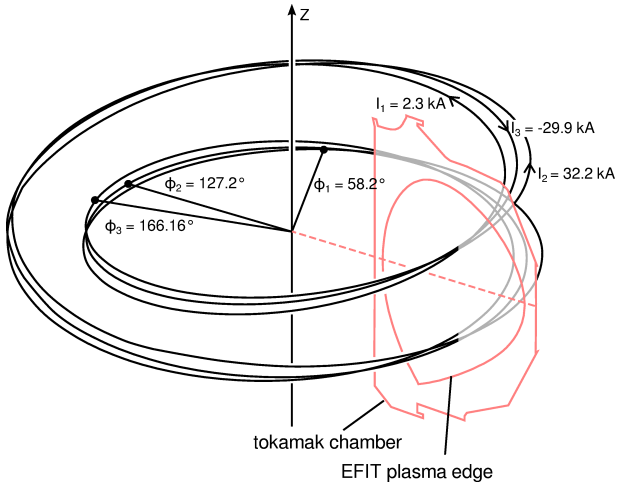

FIG. 2. The error functional is well minimized by three helical currents at the surface rotating toroidally at the measured dominant frequency 6.67Hz.

In Fig. 3 we show the comparison between the poloidal magnetic field measured by the magnetic probe at $(R, z) = (2.4, 0.0)$ m, $\phi = 97°$, and the modeled value using a Biot-Savart calculator for the same location when the sources are the filamentary currents at $q = 1$. For the modeled portion of the shot between 2700 and 3000 ms the filament currents and phases were kept constant in the rotating frame. Between 2400 and 2900 ms, the magnetic fluctuations have an approximately constant amplitude and frequency, but at the end of the heat flux measurements, after 2900 ms, the magnetic fluctuations are slightly increased.

After the parameter optimization, the filamentary currents account for the amplitude, phase, frequency and general shape of the magnetic oscillations in most of the magnetic probes signals, with some variations caused by small departures from a rigid rotation of the currents comprising the plasma response.

Now that we are endowed with a simplified description of the non-axisymmetric field in the rotating frame we can calculate the corresponding non-axisymmetric separatrix that expectedly delimits the time-dependent region of increased heat flux at the divertor targets.

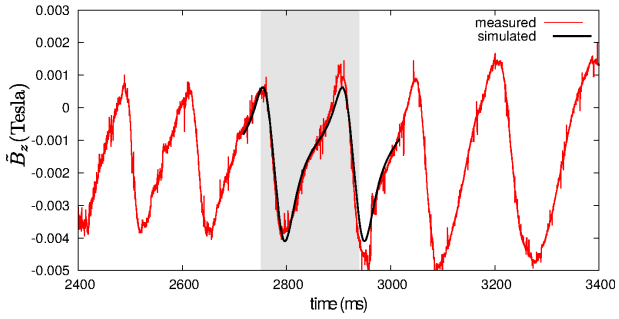

FIG. 3. Comparison between the magnetic probe signal at $\phi = 97°$ (red) from Fig. 1, and the vacuum field created by the modeled rotating internal filaments at the probe location (black). The shadowed region contain the times of the heat flux measurements in Fig.1.

B. Calculation of the magnetic separatrix

In axisymmetric situations the magnetic field lines inside the plasma span a continuous set of nested toroidal magnetic surfaces. In diverted magnetic configurations these toroidal surfaces exist inside a magnetic separatrix containing one or more X-points (magnetic saddles). More precisely, the separatrix is defined by the field lines that converge to the X-points when followed in any direction, and in most situations the separatrix is spanned by the field lines converging to a single X-point.

In the axisymmetric case, the combined X-points at every poloidal section define a circle $(R, z) = (R_s, z_s), 0 \leq \phi < 2\pi$, where the poloidal field vanishes and the Jacobian of $\vec{B}_0$ has real eigenvalues. As the magnetic field is purely toroidal, a field line starting at (R_s, z_s) is a closed circle passing through every X-point. In non-

axisymmetric situations we can say, equivalently, that the X-points are defined by a field line closing after one toroidal cycle. In the following we will refer to this field line as an Unstable Periodic Orbit (UPO)[1].

With this we can implement the definition of a separatrix for non-axisymmetric situations with an alteration. Now, the surface is defined by the field lines converging to the UPO when followed in one direction. This causes the existence of two different surfaces or invariant manifolds defining the confined region. The *unstable manifold* is spanned by field lines converging to the UPO when followed opposite to the field direction, and, conversely, the *stable manifold* is spanned by the field lines converging to the UPO when followed in the direction of the field. Both surfaces are infinite and non-self-intersecting, but can intersect each other in very intricate patterns. The set of orbits converging to the UPO when followed in any direction lie on the intersections of the stable and unstable manifolds, referred to as homoclinic points, and they do not span a continuous surface, i.e. there are gaps between these orbits and they can not be the generalization of the axisymmetric separatrix.

In non-axisymmetric situations the UPO is a global structure and can not be identified using only local information. This happens because the toroidal angle ϕ is no longer a cyclic coordinate, i.e. the vanishing of the poloidal magnetic field can not be used to determine the UPO. To locate this orbit we need to identify the fixed point of the Poincaré Map $\tilde{P}$, at a given plane transverse to the magnetic field (see Appendix). Once identified this point it can be used to build the UPO by integrating the magnetic field starting at $\tilde{P}$ until it closes after one toroidal cycle.

In the neighborhood of the fixed point $\tilde{P}$, at the transverse plane, the invariant manifolds can be approximated using polynomials that adjust the behavior of neighboring field lines. Then, small segments of the manifold cuts can be mapped forward or backwards to build the rest of the manifold cuts far from the UPO. The MAGMAN routine provides an adaptive calculation of this manifold cut by introducing new orbits *on the fly* avoiding redundant calculations and spurious points, resulting in a well spaced sequence of linkable points that represent the invariant manifold intersection with the transverse plane (see Appendix).

Using the methods described in the Appendix, we were able to identify the intersection of the UPO with the plane $\phi = 0$ for the equilibrium perturbed by the three filamentary currents in Fig. 2. The fixed point was located at $(R_s, z_s) = (1.3798, -1.0618)$ m, at approximately 6 mm from the unperturbed saddle $(R_s^0, z_s^0) = (1.3816, -1.0672)$ m. Then we calculated the intersection of the invariant manifolds with the poloidal plane at $\phi = 0$ using the adaptive advection of elementary segments.

In Fig. 4, we show the cut of the invariant manifolds at $\phi = 0$ in the rotating frame, where the helical filaments are stationary. The invariant manifolds develop the characteristic *homoclinic lobes* [1] created by the magnetic perturbation on the invariant manifolds as they get stretched and folded to preserve the toroidal magnetic flux. The multiple intersections of the invariant manifolds lead to the proliferation of UPOs of higher periods by the *horseshoe mechanism* [14] which drives the chaotic behavior of the field lines at the plasma edge.

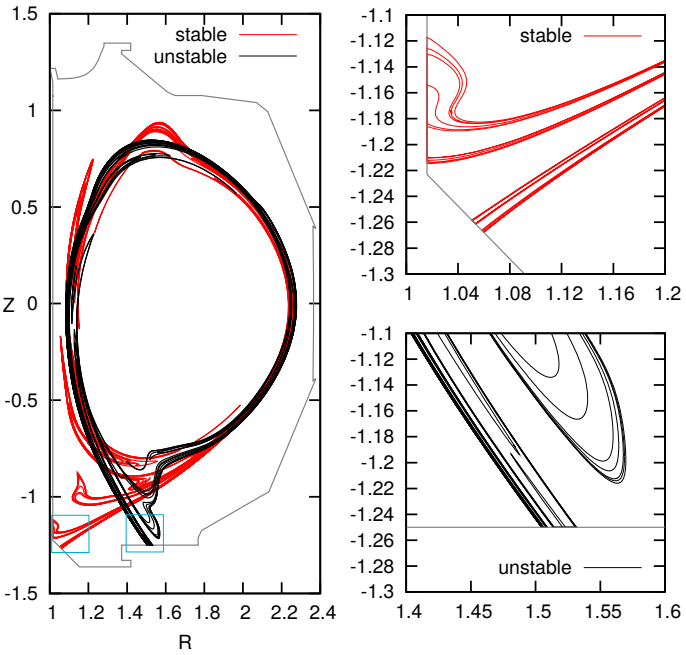

FIG. 4. Cut of the invariant manifolds in the plane for discharge #158826 subjected to the non-axisymmetric field created by three helical filaments at the surface $q = 1$. The detail of the manifold intersection with the chamber reveal the layered interior of the magnetic footprints.

IV. RESULTS AND DISCUSSION

As we move toroidally in the rotating frame, (or as the time advances in the laboratory frame), the lobes move towards the UPO, and get stretched and folded. During the stretching, the invariant manifold crosses the tokamak wall in several regions that rotate toroidally in the laboratory frame.

These crossings can be calculated with MAGMAN in the same way that the continuous poloidal section was calculated. The manifold cut at the tokamak chamber delimits the magnetic footprints or escape patterns and defines the internal boundaries through which there are abrupt changes in the connection lengths in a laminar plot.

To compare the calculated manifolds in the rotating frame with the heat deposition patterns measured at a fixed location in the laboratory we need to transform the times of the heat measurements to the corresponding toroidal phases of the rotating frame. This is achieved

by

$$\phi_i' = \phi_c - \Omega(t_i - t_0), \tag{5}$$

where t_i is the time of the i'th measurement, ϕ_c is the toroidal phase of the IR camera, and $\Omega = 2\pi \times 6.67$ Hz was determined from the waveforms captured by the magnetic probes.

In Fig. 5 we depict the intersection of the unstable manifold with the chamber wall for the LFS strike region in the rotating frame. Overlapped on the manifold in this figure, we depict the corresponding experimental heat flux measurements depicted in Fig. 1 at the corresponding phases in the rotating frame for the time of each heat flux profile.

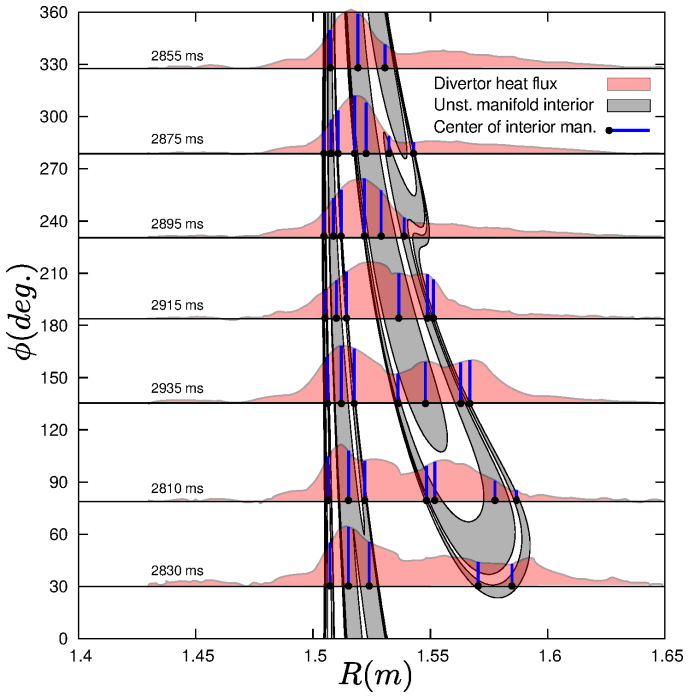

FIG. 5. The unstable invariant manifold intersecting the DIII-D divertor plates in discharge #158826 in a rotating frame with toroidal frequency of 6.67 Hz (solid black lines and manifold interior in gray), and an overlay of the experimental heat flux measurements for the corresponding toroidal phases of the rotating frame (profiles in light-red). The heat flux peaks are well correlated with the center of the manifold interior (blue lines) for most phases, and the secondary heat flux peak disappears where the lobes get too close radially to be resolved by the IR camera. The heat pattern repeats periodically, as expected if the manifold rotates rigidly.

Notice that the heat flow peaks match reasonably well with the manifold interiors, and the observed peak splitting agrees well with the multiple interiors for each toroidal phase of the rotating frame. As discussed before, the invariant manifolds delimit the volume of confined field lines in non-axisymmetric situations. Consequently, the field lines inside the manifold can access the plasma interior driving the hot plasma by parallel transport to the Plasma Facing Components (PFC), while the field lines outside the manifold can not access the plasma and will only drive particles that leave the manifold interior by cross-field transport, which is small compared to the parallel transport.

It is interesting to notice that, for $240° < \phi < 360°$, the camera sees a single heat peak moving from $1.52m$ to $1.525m$, which is well aligned with the clustered lobes, but as the lobes get separated the peak splits and the main peak moves to the HFS following another piece of the manifold with a smaller radial extension. Clearly, the heat load is not aligned with the axisymmetric strike line from EFIT at $R = 1.5$ m but follows the wider lobes. This behavior explains the small misalignment between the HFS flux peak and the strike point position from the axisymmetric reconstruction in Fig. 1. This measurement is consistent with the invariant manifold delimiting the region of enhanced heat flux in non-axisymmetric discharges and indicates that the heat flux may be concentrated in the lobes instead of the region where the manifold gets compressed near the unperturbed axisymmetric strike line.

An important point is that the calculation of the manifold interior is not intended to describe the heat flux profile, but to identify the regions of the chamber affected by parallel transport. To describe the profile features as width and peak locations and number of peaks a transport simulation that include particle drifts would be required, but it is interesting to notice that the plasma edge calculation through invariant manifolds explains well the radial extension of the heat load and approximates well the locations of the main peaks.

The identification of the invariant manifolds with the plasma edge brings interesting possibilities for the interpretation and modeling of plasma structures near the plasma-vacuum interface and the evolution of the heat loads on the chamber components. These structures may emerge from parallel transport along the field lines resulting from the overlapping of dynamic and stationary magnetic fields in the presence of a magnetic saddle. This general situation may be relevant during the ELM suppression by Resonant Magnetic Perturbations where a non-stationary magnetic perturbation caused by evolving currents in the plasma is combined with an externally applied magnetic perturbation. Also, the so-called filamentary structures may be a manifestation of time-dependent helical features developing at the invariant manifolds [15], but this may require more detailed modeling of the non-axisymmetric source currents.

V. CONCLUSIONS

In this work we have shown that the non-stationary non-axisymmetric field created by internal time-dependent currents leads to the evolution of the invariant manifolds that delimit the region of confined field lines in a tokamak discharge. This evolution has

measurable effects in the strike region that changes according to the phase of the internal sources of asymmetric field and matches well with the measured heat flux from the IR camera. This matching was obtained for a minimalist model of three helical filamentary currents in the $q = 1$ surface without externally created magnetic perturbations. A more sophisticated treatment involving several rational surfaces, more filamentary currents and the externally produced magnetic perturbations can provide more details of the heat patterns and the topological changes experienced by the manifolds, but in terms of experimental observations a simple model with reasonable proportions gives a good quantitative match. The study of the interplay between internal currents and the magnetic topology may provide an important insight on the nature of coherent structures developing at the plasma edge, since these have some characteristic properties of time-dependent invariant manifolds.

ACKNOWLEDGMENTS

This work has been supported by Brazilian scientific agencies CAPES, CNPq and the São Paulo Research Foundation (FAPESP) under grants 2011/19269-11, 2012/18073-1 and 2014/03899-7, and by the U.S. Department of Energy, Office of Science, Office of Fusion Energy Science under DOE awards: DE-FC02-04ER54698, DE-SC0012706 and DE-FG02-05ER54809. The authors wish to thank Dr. Michael A. Makowski for his help on interpreting the heat flux data.

VI. APPENDIX

A. Unstable Periodic Orbits and Invariant Manifolds

To localize the Unstable Periodic Orbit (UPO), or saddle orbit, let us introduce the Poincaré map $M : S \to S$, where S is a given surface, for instance $\phi = \text{const.}$, which is always transverse to the magnetic field, and $M(P)$ is the position of a field-line starting at $P \in S$ after one toroidal transit in the direction of the field (Fig. 6). The inverse map M^{-1} is obtained when we follow the line in opposite direction to the field. Notice that, $M(M{-}1(P)) = M^{-1}(M(P)) = P$.

The explicit form of M is unknown and we can only calculate it numerically through the integration of the field lines. The field line tracing is performed with an order five adaptive Runge-Kutta integrator [16]. The error estimate was adjusted to 10^{-12} m per step, so that, cumulative errors are expected to be small.

Formally, we can look for the fixed point P satisfying $M(P) = P$, which belongs to the UPO (Fig. 6). This can be accomplished numerically using a Levenberg-Marquardt algorithm [13] with a tracking stage or the Broyden's method [17]. Both methods involve the approximation of the Jacobian matrix of M using finite differences. Provided a good initial guess of P the method converges in few iterations, usually, less than 10. For a perturbed single-null discharge the unperturbed saddle becomes good initial for the UPO.

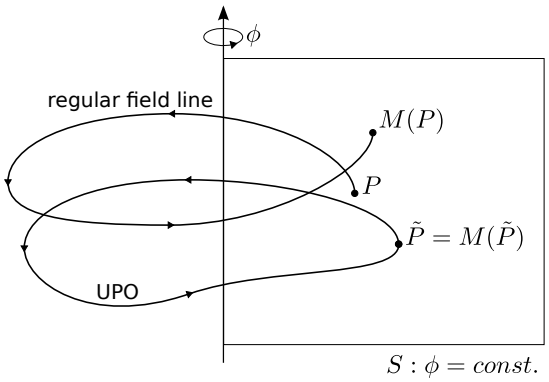

FIG. 6. Intersections of a regular field line and the UPO with a Poincaré plane.

In the neighborhood of the fixed point $P \in S$ the invariant manifolds dominate the geometry of the field lines (Fig. 7). A localized set of points around P will be stretched along the unstable manifold as we apply the Poincaré map M repeatedly, and the same set of points will be stretched along the stable manifold upon repeated applications of M^{-1}.

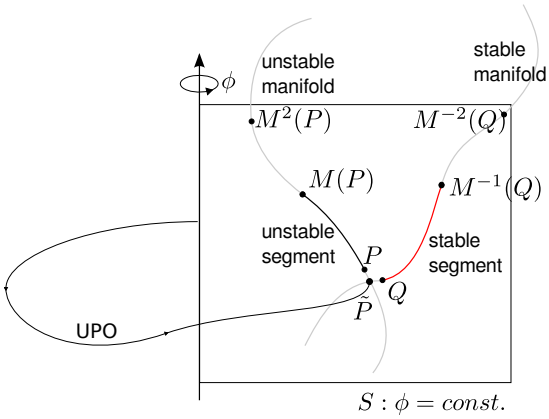

FIG. 7. The invariant manifolds are calculated by applying the Poincaré map to small segments of the invariants close to the UPO. The local invariants are obtained by fitting the mapped points from a neighborhood of $\tilde{P}$.

To only visualize the manifold cut it is sufficient to initialize a large number of points around $\tilde{P}$, and apply repeatedly the map or its inverse respectively. However, this method results in a scattered representation of the manifold, which can not be optimized in a controlled fashion and can not be generalized to represent the manifold in three-dimensions, which may be desirable for comparison with tangential imaging of the plasma

edge. In this work we use the local behavior of the field lines around $\tilde{P}$ to calculate a local representation of the manifolds by adjusting a set of stretched points with a polynomial of order 5 or 7 containing the fixed point for both the stable and unstable manifolds. Then we use an adaptive algorithm to build the rest of the manifold in the transverse surface S.

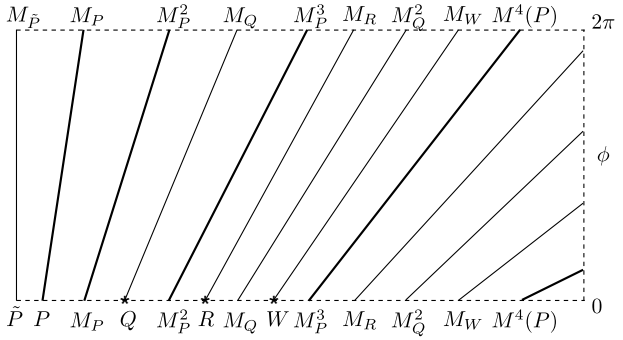

FIG. 8. Representation of the optimization process. Each line represents a field line on the invariant manifold. At the top and bottom we have the intersections with the Poincaré plane $\phi = 0$, where $M_P^N = M^N(P)$. After the first cycle, the distance between M_P and M_P^2 was larger than the critical distance d_c, then a new orbit is created at Q. The refinement continues, by measuring the distance between M_P^2 and M_Q that is also larger than d_c, originating R and so on. The starting points of the new orbits are calculated in the cutting plane using Lagrange polynomials passing through the neighboring points.

For this task we use the MAGMAN routine, which consists in applying the Poincaré map repeatedly to a local segment of the manifold around $\tilde{P}$ (Fig. 7). The spatial resolution of the manifold is preserved by means of a refinement procedure that enables the introduction of new field lines where they are needed (Fig. 8), avoiding the introduction of new orbits very close to $\tilde{P}$ and preventing the clustering of points in other regions of the manifold. This method uses the points describing the manifold segment in the previous iteration to calculate new initial conditions at the places where the distance between consecutive points becomes larger that some critical distance d_c. This critical distance was estimated by requiring that the lobes were well resolved. For this, we estimated the characteristic lobe size and required it to be one order of magnitude larger that d_c.

The new points are calculated with Lagrange polynomials at the cutting surfaces to insert the required new orbits smoothly within the sequence of existing ones. The MAGMAN routine is similar to the MAFOT about the propagation of local segments [12], but differs in the dynamic refinement of the segment. MAGMAN also allows us to continue the manifold along material objects, like the divertor tiles and the vacuum chamber without extra calculations or resolution loses, also, it returns an organized sequence of points that can be connected with segments to represent the manifold.

To illustrate the importance of having an organized and well distributed sequence of points we calculate the invariant manifolds of the EFIT equilibrium reconstruction for the shot #158826, when subjected to an external $n = 3$ perturbation. For comparison, we represent the manifolds by mapping a set of 7500 random initial conditions close to the UPO for 9 toroidal cycles. In Fig. 9 we compare the resulting scatter plots from the random sampling with those from MAGMAN, which in addition are organized and can be joined smoothly.

The comparison is performed so that the number of points representing the manifold in the random and adaptive calculations is the same. For the presented results, the MAGMAN calculation requires only 10% of the mappings required by the random sampling method and involves only 5% of its integration steps and computation time, this happens because the lobes of the manifold develop in regions where the adaptive step integrator performs larger steps. If the comparison is performed so that we obtain the same quality representation with both methods the number of random initial conditions must be tripled, and the number of required mappings for the random method will be 30 times the required by MAGMAN. Consequently, the computation time would be about 60 times the required by MAGMAN for a plot with the same quality.

[1] Guckenheimer J and Holmes P 1983 *Nonlinear Oscillations, Dynamical Systems and Bifurcations of Vector Fields* (Springer - Verlag)

[2] da Silva E C, Caldas I L, Viana R L and Sanjuán M A F 2002 *Phys. Plasmas* **9** 4917

[3] Roeder R K W, Rapoport B I and Evans T E 2003 *Phys. Plasmas* **10** 3796

[4] Evans T E, Roeder R K W, Carter J A, Rapoport B I, Fenstermacher M E and Lasnier C J 2005 *J. Phys. Conf. Ser.* **7** 174

[5] Kirk A, Harrison J, Liu Y, Nardon E, Chapman I T, Denner P and (the MAST team) 2012 *Phys. Rev. Lett.* **108** 255003

[6] Pompherey N and Reiman A 1992 *Phys. Fluids B-Plasma* **4** 938

[7] Volpe F A G, Austin M E, Haye R J L, Lohr J, Prater R, Strait E J and Welander A S 2009 *Phys. Plasmas* **16** 102502

[8] Buttery R J, Hender T, Ashall J, Blow K A G and Fielding S 1996 *Nucl. Fusion* **36** 1369

[9] Lao L, John H S, Stambaugh R, Kellman A and Pfeiffer W 1985 *Nucl. Fusion* **25** 1611

[10] Cahyna P, Nardon E and Contributors J E 2011 *J. Nucl. Mat.* **415** S927

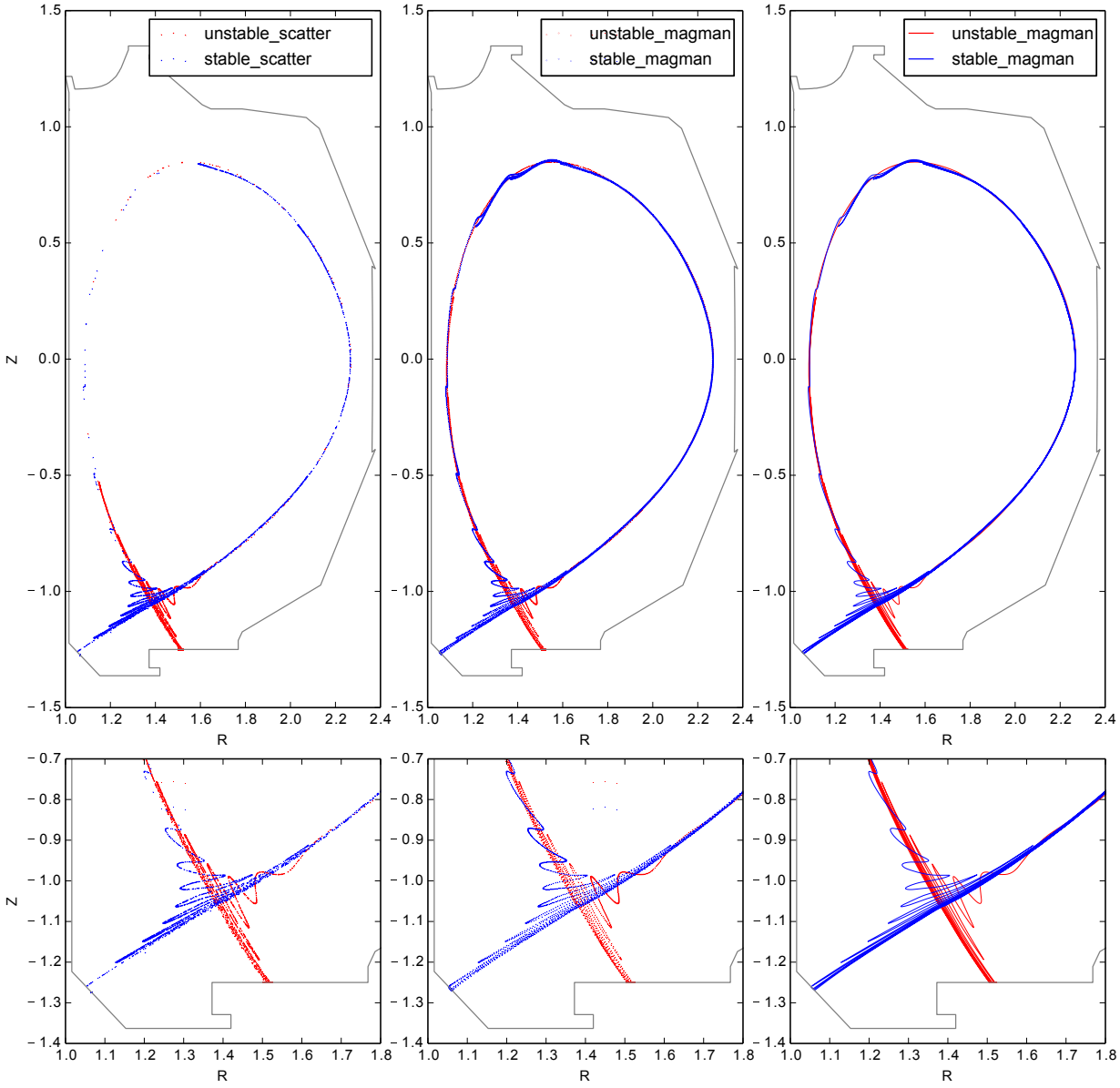

FIG. 9. The left column shows the scatter-plot of a set of 7500 random initial conditions close to the UPO mapped for 9 toroidal cycles. The center column shows the scatter plot of the MAGMAN adaptive calculation, with the same number of points. Clearly, the MAGMAN points are better distributed along the manifold and reach farther regions. The third column shows the smooth line traced along the organized MAGMAN points. As the random sampling does not provide organized points, they can not be joined smoothly to represent the manifold.

[11] S R H and Nakajima N 2010 *Phys. Plasmas* **17** 052511
[12] A Wingen T E Evans K H S 2009 *Nucl. Fusion* **49** 055027
[13] Marquardt D W 1963 *SIAM J. Appl. Math.* **11** 431
[14] Smale S 1967 *B. A. Math. Soc.* **73** 747
[15] Eich T, Herrmann A, Neuhauser J and Team A U 2003 *Phys. Rev. Lett.* **91**
[16] Cash J R and Karp A H 1990 *ACM T. Math. Software* **16** 201
[17] Broyden C G 1965 *Math. Comp.* **19** 577